AIAA JOURNAL
Vol. 47, No. 2, February 2009

Two-Dimensional Visualization of Turbulent Wall Shear Stress Using Micropillars

S. Große* and W. Schröder†
RWTH Aachen University, 52062 Aachen, Germany

DOI: 10.2514/1.36892

The wall shear-stress sensor MPS³ based on flexible micropillars has been used to experimentally assess the two-dimensional wall shear-stress distribution in turbulent duct flow at moderate Reynolds number. The sensor covers an area of 90 × 125 viscous length scales along the streamwise and spanwise directions, respectively. Applying Taylor's hypothesis allows a further increase in the streamwise extension. Preliminary results evidence the coexistence of low- and high-shear regions representing footprints of near-wall coherent structures. The low-shear regions resemble long meandering bands interrupted by local high-shear-stress regions. A qualitative comparison evidences the structures detected in the present study to be similar to wall shear-stress distributions reported in the literature and to structures found in higher regions of the boundary layer. These preliminary findings indicate the potential of the micropillar sensor concept to be capable of detecting the multidirectional planar wall shear-stress distribution in turbulent flows. A detailed discussion of the wall shear-stress characteristics and of the geometric properties of the streaklike structures is beyond the scope of this paper, and a more intrusive discussion needs to be done in the future.

Nomenclature

f	=	frequency, Hz
H	=	channel height, m
L_p	=	pillar length, m
l^+	=	viscous length scale
Re_{cl}	=	Reynolds number based on H and U_{cl}
Re_H	=	Reynolds number based on H and U_b
Re_τ	=	Reynolds number based on H and u_τ
T_b	=	time scale based on bulk/outer variables H and U_b
T^+	=	time scale based on inner variables u_τ and ν
u	=	streamwise velocity, m/s
u_τ	=	friction velocity, m/s
U_b	=	bulk velocity, m/s
U_c	=	convection velocity, m/s
U_{cl}	=	centerline velocity, m/s
x, y, z	=	streamwise, wall-normal, spanwise coordinates, m
η	=	dynamic fluid viscosity, kg/m/s
ν	=	kinematic fluid viscosity, m^2/s
ρ	=	fluid density, kg/m^3
τ	=	wall shear stress, N/m^2
$\bar{\tau}$	=	mean wall shear stress, N/m^2
τ'	=	wall shear-stress fluctuation, N/m^2

Superscript

$+$	=	viscous scales

I. Introduction

THE wall shear stress $\tau_{\mathrm{wall}} = \eta \cdot \partial u/\partial y|_{\mathrm{wall}}$ results from the relative motion between the wall and the fluid. The determination of wall shear stress is of utter importance in turbulence research. The mean wall shear stress defines the friction velocity $u_\tau = \sqrt{\tau_{\mathrm{wall}}/\rho}$, which is relevant to determine nondimensional variables such as u^+ or y^+. Thereby is the friction velocity u_τ assumed to serve as one of the most fundamental scaling parameters in turbulence. However, there is still debate as to what extent turbulence actually scales with u_τ, but its determination to within high accuracy would bring progress to this question [1,2].

The fluctuating wall shear stress and its spatial distribution are direct indicators of the dynamic behavior of near-wall turbulent structures, and this knowledge gives insight into the turbulent momentum transfer processes in the proximity of the wall and is, as such, of fundamental importance for the basic understanding of their mechanics. Many experimental and numerical studies in the past concluded from their findings that only a spatially distributed view of the flowfield in its instantaneous and in its statistical representation will allow for a better comprehension of the highly nonlinear processes involved in the self-sustaining processes of turbulence production and conservation in turbulent shear flows. In this sense, the micropillar shear-stress sensor MPS³ serves as a useful method to detect the footprints of structures at higher regions in the shear flow (e.g., in the buffer region) to complete the image of the vortical flowfield even down to the wall on which many experimental techniques, and especially spatially and temporally resolved techniques, have failed.

Investigations of turbulent shear layers performed by [3–6] showed the coherent turbulent structures, which have been found in different regions of turbulent shear layers, to strongly meander in the spanwise direction when they convect along the streamwise direction. Similar findings have also been observed for the wall shear-stress distribution in the present studies. Keeping in mind the meandering feature of the large-scale motions, it is natural to suppose that single-point statistics tend to mask the true length of these turbulent structures. This problem has already been noticed by [7], who found the streamwise length scales derived from streamwise velocity gradient fluctuations near the wall (i.e., wall shear-stress fluctuations) to reach $x^+ = 1200$ and who considered this to be only the minimum extent of the near-wall streaks, due to their meandering or moving downstream under acute angles. Therefore, the multipoint assessment of the spanwise wall shear-stress distribution will allow further investigation of this aspect.

The measurement of the streamwise wall shear-stress distribution would further allow investigation of how far Taylor's hypothesis of frozen turbulence [8] is suitable to estimate the spatial distribution even in highly fluctuating regimes of turbulent boundary layers.

Received 28 January 2008; revision received 22 September 2008; accepted for publication 5 October 2008.

*Research Scientist, Institute of Aerodynamics; currently Laboratory for Aero- and Hydrodynamics, Delft University of Technology, The Netherlands; s.grosse@aia.rwth-aachen.de (Corresponding Author).

†Head of Institute of Aerodynamics.

Although this aspect has already been addressed in the literature [9], the discussion was so far based on numerical data, and it should be kept in mind that the periodic computational domain of finite length and width in which the numerical simulations are performed will also impact the spacial length scales and thereby Taylor's hypothesis. Therefore, there is still a great demand of simultaneously acquired time- and space-dependent data.

Furthermore, the measurement of the skin friction is essential in many technical applications (e.g., in the field of drag reduction and performance enhancement for transportation vehicles) in which the viscous surface drag plays a major role. In flow control applications, the assessment of the local wall shear stress or of the wall shear-stress distribution is a necessary prerequisite for the formulation of low-dimensional control models. The spanwise wall shear-stress fluctuations have been especially evidenced to serve as an efficient control loop parameter in the context of drag-reducing flow control [10,11]. The exact relationship between the spanwise wall shear-stress fluctuations and the achieved drag reductions is still unknown, and only a detailed investigation of the near-wall turbulent processes will lead to an improved understanding of the complex relationships and might further yield advancements in flow control applications. Again, to fully understand the intricate changes in turbulent structures responsible for drag reduction, it will be necessary to assess the two-dimensional wall shear-stress distribution and to capture individual changes in space and time in detail, rather than to only concentrate on integrational or statistical changes, which might eventually be masked by the aforementioned drawbacks of single-point techniques. Note, however, that the micropillar sensor principle at the current state does not allow for a real-time evaluation of the wall shear stress, as would be necessary for such a flow control application. However, the micropillar shear-stress sensor MPS^3 with its multidirectional sensitivity is predestined to further investigate the nonlinear processes and might, as such, play an important role in an optimization of the model-building processes for flow control applications.

Furthermore, the local wall shear stress can be applied for the modeling of the wall condition in high-Reynolds-number large eddy simulation (e.g., [12]). Here, the temporal and spatial development of the wall shear-stress distribution would be of especially great interest.

Despite the variety of different sensor designs that have been proposed in the literature, it can be stated that the multidirectional (i.e., streamwise and spanwise) determination of the planar wall shear-stress distribution, which has been shown in the preceding discussion to be of essential interest in theoretical and applied fluid mechanics, is still an open issue in the field of experimental fluid mechanics, and to the knowledge of the authors, the only literature that has reported on the planar wall shear-stress distribution is that of [13–15], who applied spanwise-aligned wall-mounted hot-wire sensors to assess the wall shear-stress distribution in a turbulent shear layer.

A first qualitative application of the micropillar shear-stress sensor MPS^3 in turbulent flow is described in this paper to evidence the potential of the technique to detect the two-dimensional wall shear-stress distribution. The sensor consists of flexible micropillars, which protrude into the viscous sublayer and which bend in reaction to the exerted fluid forces. The deflection of the pillar tip is detected optically and serves as a representative of the local wall shear stress. The pillar sensor is statically calibrated in linear shear flow and possesses a flat dynamic response up to several hundred hertz, such that the turbulent fluctuations at the Reynolds numbers in the experiments can be captured at a constant gain.

Note that, in general, it is possible to apply the sensor to reverse flowfields. However, it still needs to be determined how far the linearity of the velocity field in the viscous sublayer, on which the quantitative evaluation of the wall shear stress by means of micropillars is based, is still valid in regions of separated flow or flow reversal. However, the pillar technique should be a suitable technique to at least qualitatively determine the characteristics of these flowfields. The sensor principle has already been described in great detail in [16–18], and the reader is referred to these publications for further information.

In the following section, the flow facility and details of the micropillar sensor setup are briefly described. Then the results of the wall shear-stress measurements will be presented, and some conclusions will then be drawn.

II. Flow Facility and Experimental Setup

The experiments were performed in a duct flow facility (Fig. 1a). The measurement section with square cross section possesses a hydraulic diameter $H = 42$ mm. A schematic of the measurement section and a definition of the coordinates is depicted in Fig. 1b. The fluid used in the measurements is deionized water at 20 ± 0.1°C. The Reynolds number based on the bulk velocity $Re_H = U_b H/\nu$ is calculated from the measured volume flux V, which can be determined to within 0.3% accuracy. The wall shear-stress measurements have been performed at $Re_H = 15,000$, which corresponds to a Reynolds number based on the friction velocity of $Re_\tau = u_\tau H/\nu$ of 900.

The flow enters through a flow straightener with a 5 mm core size, followed by a 0.2 mm fine mesh. The straightener is connected to a 1-m-long ($25H$) duct section, with a tripping device for fixed transition at the end. For fully developed turbulent duct flow, the measurements are performed another 1 m ($25H$) downstream of the tripping edge [19] . The tripping device consists of a ring with a rectangular cross section, generating a contraction ratio of 0.85, in which the contraction ratio is defined as the ratio between the cross section in the contraction and that of the duct. The fluid exits the measurement section into an open reservoir and flows through a heat exchanger to maintain a constant fluid temperature. Particle-image velocimetry (PIV) measurements recorded with 1000 samples at 2 Hz at Reynolds

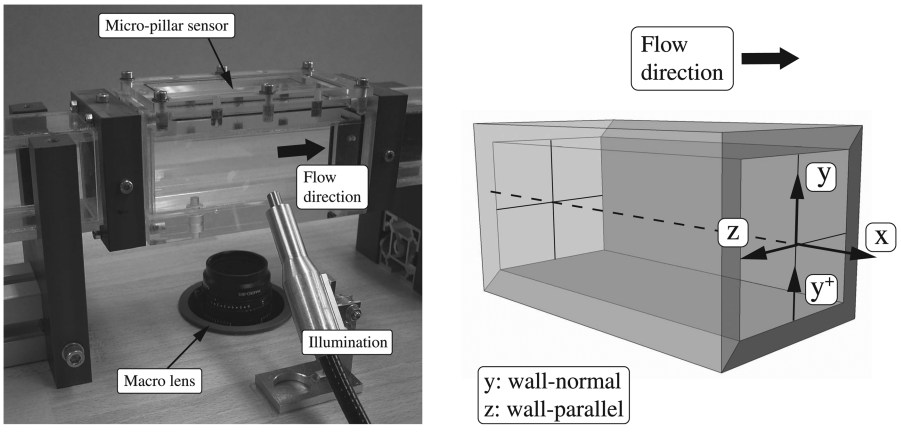

a) b)

Fig. 1 Images of the a) experimental setup and b) measurement section with a definition of the coordinates.

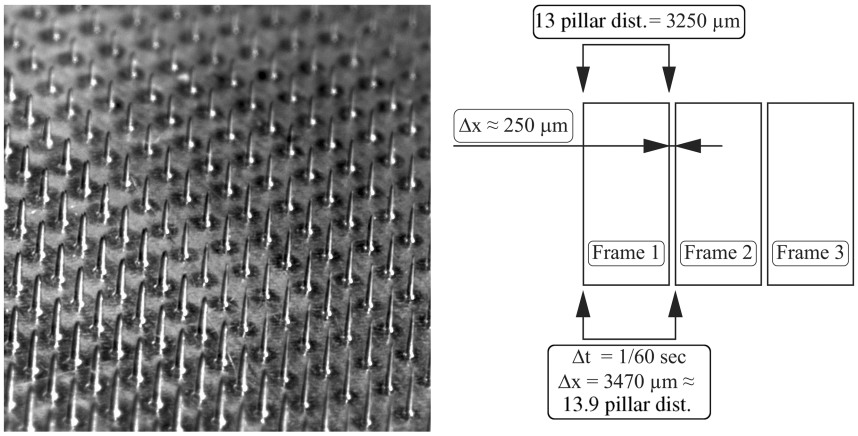

a) b)

Fig. 2 Images of a) pillar array similar to that used in this study and b) sequential recombination of frames in the present study.

numbers Re_H ranging from 5000–20,000 and pressure-drop measurements confirm the statistical properties of fully developed turbulent duct flow in the measurement section and show good consistency with numerical results from the literature [20–22].

The micropillar sensor array consists of 17×25 pillars in the streamwise and spanwise directions, respectively, and is mounted flush in the duct wall. The lateral spacing of 250 μm corresponds to approximately 5.3 viscous units. An array of micropillars similar to that used in this study is shown in Fig. 2a. The micropillars have a height L_p of approximately 160 μm, corresponding to about 3.4 viscous units at the Reynolds numbers in the experiment, ensuring that the sensor structure is completely embedded in the viscous sublayer of the duct flow. Note that this is essential to ensure that the sensor experiences a linear velocity gradient. The sensor displacement from a reference position at no velocity is observed using a macrolens mounted on a Photron Fastcam 1024 PCI high-speed camera.

Great care was taken to ensure that no additional disturbance arises from the mounting of the sensor. The temperature is kept constant during calibration and the duct measurements such that a possible temperature drift can be kept within $\pm 0.25\%$. Under the given experimental conditions, the sensor evidences no acceleration or pressure-gradient sensitivity. Furthermore, due to its symmetric shape and the optical detection principle, the sensor does not experience cross-axis sensitivity and, as such, allows the multidirectional detection of the wall shear stress in magnitude and angular direction. Experiments with generic and experimental data, which have been performed to test the uncertainty in the evaluation of the pillar-tip deflection, evidenced the accuracy of the image-evaluation routines to be within 0.03 pixels at the achieved image quality. Note that modified PIV correlation routines are used to determine the pillar-tip deflection. This rms level can be considered as the noise level of the entire sensor system.

Note that to detect the pillar deflection at a high enough accuracy, it is necessary to adapt the optical setup such that pillar deflections in the order of several pixels can be recorded. However, the optical resolution and the geometry of the structures in this study caused the mean[‡] displacement of the detected pillar tip on the charge-coupled device to be 0.7–0.8 pixels. With the achievable accuracy in the optical detection of the pillar tip, the detection error is about 4%. However, some of the sensor posts were defective (this is also evidenced in Fig. 5, in which single spurious vectors can be identified). Note that under optimum conditions, an accuracy in the sensor detection of up to 0.5% can be achieved.

The camera is operated at $f = 60$ Hz. Although the recording frequency is not high enough to detect the highest turbulent frequencies, which have been estimated to be approximately 250 Hz at the Reynolds number in the experiments, the large-scale structures can well be resolved. Only 512 images have been recorded in this feasibility study, due to the limited available camera memory, resulting in a total recording period of 8.5 s. During this time span, a particle with bulk velocity U_b travels a distance of approximately $70H$, which is insufficient for a proper statistical analysis of the data. This aspect will be briefly addressed in the following.

[‡]Here, *mean* cannot be considered to be a converged mean wall shear stress from a fluid mechanics point of view due to the short measurement time. *Mean* only refers to a medium value of the wall shear stress during the measurement.

III. Results

A. General Remarks

Note that the present data do not allow for a proper investigation of the characteristics of turbulent wall shear stress from a fluid mechanics point of view, due to the insufficient time span of the recordings. As mentioned earlier, the time span of the measurements only corresponds to 70 bulk-time scales based on the duct height H and the bulk velocity U_b, such that the certainty to which statistical properties such as turbulence intensities, probability density function (PDF) of the fluctuations, and two-point correlations can currently be given is reasonably low [23]. Therefore, the measurements reported in the context of this paper should rather demonstrate the general feasibility of the multidirectional detection of the two-dimensional wall shear-stress distribution in turbulent flows using the MPS[3] sensor technique. Thus, a quantitative discussion of the data is beyond the scope of the present paper, and measurements over larger time spans with more data samples, which will be performed in the near future, will be necessary to allow for an adequate database for a reliable statistical investigation.

Furthermore, the wall shear-stress data discussed in the following have, strictly speaking, been recorded at turbulent duct flow and should not be considered representative for two-dimensional channel flow, which is often referred to in fundamental turbulence research. Nonetheless, it goes without saying that turbulent phenomena of both channel and duct flows should at least be similar.

B. Taylor's Hypothesis of Frozen Turbulence

Although the spanwise width of the near-wall coherent structures can well be captured with the sensor, the dimension in the streamwise direction exceeds the field of view of the sensor geometry. It is well known that the near-wall large-scale structures (i.e., low-speed and high-speed streaks) are reported to attain a length of approximately $1000\,l^+$. Therefore, Taylor's hypothesis of frozen turbulence [8] has been applied to estimate the sensor length in the streamwise direction. A constant convection velocity $U_c = 10 \cdot u_\tau$ [24] has been used to transform the temporal information into a spatial resolution along the streamwise axis. At the relatively low recording frequency of $f = 60$ Hz, the structure convects $U_c/f = 3.5 \times 10^{-3}$ m in the streamwise direction (i.e., about $l^+ = 75$). Applying Taylor's hypothesis on the shear-stress data of a single spanwise sensor line, a

total field of view in the streamwise direction of approximately 38,000 l^+ could be achieved with the available data.

The spatial distance of $l^+ = 75$ between two consecutive temporal frames corresponds very well to the streamwise span of 15 sensor lines (i.e., $14 \times 2.5 \times 10^{-4}$ m). As such, the information of 14 pillars in the streamwise direction has been evaluated, leading to an increased spatial resolution in this direction of 5.33 l^+. A schematic of the data reconstruction is given in Fig. 2b.

C. Preliminary Wall Shear-Stress Statistics

Preliminary results of the intensity of the streamwise and spanwise wall shear-stress fluctuations are $\tau_{x,\mathrm{rms}}/\bar{\tau}_x = 0.36$ and $\tau_{z,\mathrm{rms}}/\bar{\tau}_x = 0.17$, respectively. Thereby, the values are of the order of values reported in the literature for the limiting behavior of the velocity field in the vicinity of the wall [1,20,25,26].

The probability density distribution of the normalized streamwise wall shear-stress fluctuations $\tau_x'/\tau_{x,\mathrm{rms}}$ is given in Fig. 3a and that of the spanwise fluctuations $\tau_z'/\tau_{z,\mathrm{rms}}$ is given in Fig. 3b. The results from the present study at $Re_H = 15,000$ show good agreement with the findings of [15] at similar Reynolds numbers based on the centerline velocity and the channel height ranging from $Re_{\mathrm{cl}} = 17,600$ to 35,000 and [27] at $Re_{\mathrm{cl}} = 6600$ in channel flow. Note that the PDF of the normalized streamwise wall shear-stress fluctuations $\tau_x'/\tau_{x,\mathrm{rms}}$ is reported to be independent of the Reynolds number. The values of the skewness $S_{\tau_x} = 0.95$ and of the flatness $F_{\tau_x} = 4.47$ of the PDF are in good agreement with data reported in the literature. Note, however, that there is great scatter in the reported values.

The values of the higher-order moments of the spanwise fluctuations are for the skewness $S_{\tau_z} = 0.07$ and for the flatness $F_{\tau_z} = 5.46$. Similarly, [25] found the flatness of the spanwise velocity fluctuations in the viscous sublayer of turbulent channel flow at $Re_H = 7700$ to be higher than that of the streamwise fluctuations. Note, however, that these authors used u_τ to normalize their plots. The skewness S_{τ_z} is close to zero due to the symmetry of the flowfield.

In Fig. 3c the spanwise distribution of the correlation of streamwise shear-stress fluctuations $R_{\tau_x\tau_x}(z^+)$ and correlations of velocity fluctuations $R_{uu}(z^+)$ from direct numerical simulation (DNS) data [21] at $y^+ \approx 5$ are juxtaposed. The comparison evidences the structural scales of the wall shear-stress distribution along the spanwise direction in the present study to be of the same order of magnitude as those in the study of [21] at similar Reynolds numbers in channel flow.

The spanwise distribution of the correlation of spanwise shear-stress fluctuations $R_{\tau_z\tau_z}(z^+)$ and correlations of velocity fluctuations $R_{ww}(z^+)$ from DNS data [21] at $y^+ \approx 5$ are juxtaposed in Fig. 3d. The experimental data decay at smaller distances along the lateral direction. This trend could not be observed in further studies at similar Reynolds numbers with higher sampling times. These studies rather confirmed the correlation function of the spanwise fluctuations to well collapse with the data of [20,21,28]. As such, the discrepancy in the present data should be attributed to the insufficient time span over which the data in the present experiments could be recorded. It is well known that statistical functions such as the correlation function or the higher-order moments of fluctuations require large amounts of recorded samples and $\mathcal{O}(3–4)$ bulk-time scales of sampling time to sufficiently converge [23,29]. Furthermore, it should be kept in mind that the relative error in the detection of the spanwise fluctuations is

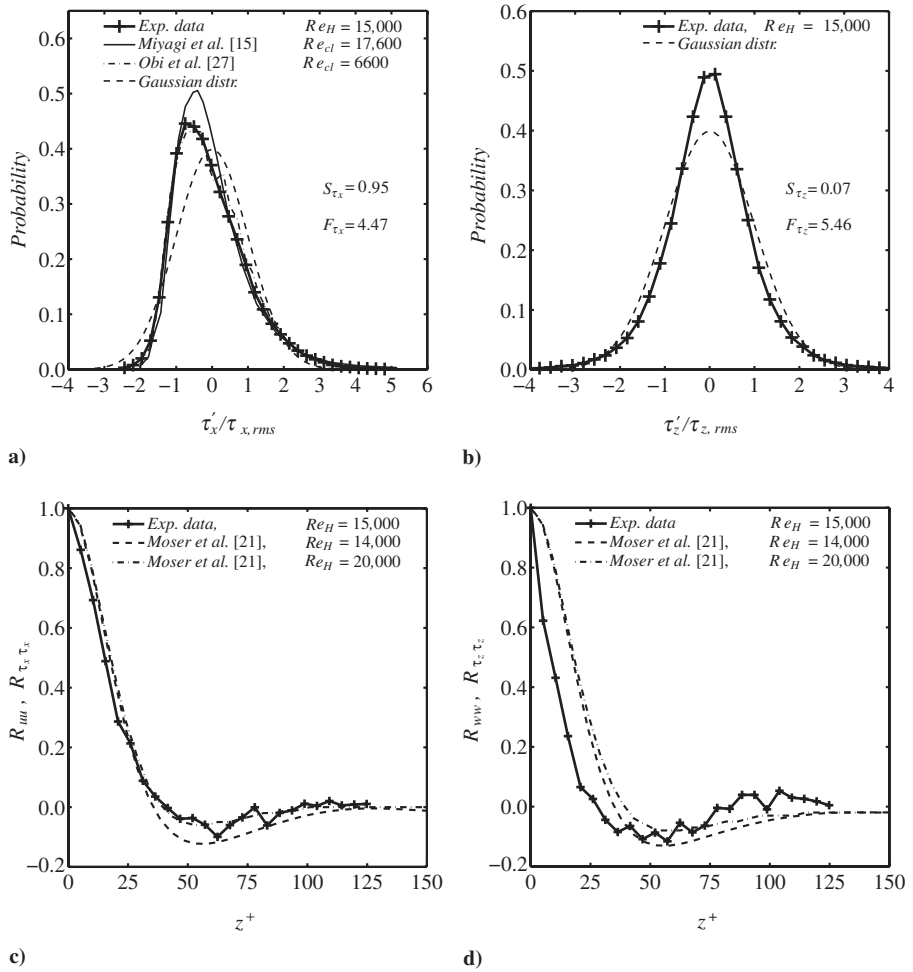

Fig. 3 Statistics of the wall shear-stress distribution: a) PDF of the streamwise wall shear-stress fluctuations, b) PDF of the spanwise wall shear-stress fluctuations, c) spanwise distribution of the correlation of streamwise fluctuations $R_{\tau_x\tau_x}$, and d) spanwise distribution of the correlation of spanwise fluctuations and $R_{\tau_z\tau_z}$

larger than that for the streamwise fluctuations, such that the correlation function for the spanwise fluctuations can be expected to be rather affected by measurement uncertainties.

The comparison of the preliminary results and those from further measurements performed over statistically sufficient time spans evidences the structural scales of the wall shear-stress distribution along the spanwise direction in the present study to be of the same order of magnitude as those in the study of [21] at similar Reynolds numbers in channel flow.

The near-wall structural features, which are represented by the turbulence statistics in the preceding discussion, should be elucidated in the following using the two-dimensional wall shear-stress distribution.

D. Wall Shear-Stress Distribution

Exemplary results of the wall shear-stress distribution are given in Fig. 4, in which each of the independent sequences has a field of view of $2500 \times 125\ l^+$ in the streamwise and spanwise directions, respectively. The contours indicate the instantaneous strength of the streamwise wall shear-stress fluctuations $\tau_x'/\bar{\tau}_x$, where $\bar{\tau}_x$ is the mean wall shear stress during the measurement.

It is evident that regions of lower and higher wall shear stresses do coexist. The low-shear regions extend over 1000 l^+ and more, being locally interrupted by high-shear regions between these structures. These distributions are supposed to be related to the very near-wall turbulent coherent structures (i.e., low-speed and high-speed streaks) aligned in and above the viscous sublayer of wall-bounded shear flows, representing one of the first evolutionary stages in the autogenerative cycle of turbulence production. It is assumed that the micropillar sensor detects the footprints of these coherent structures by measuring the local wall shear-stress distribution.

Near the wall (i.e., at $0 \leq y^+ \leq 7$), a minimum of the spanwise correlation (Figs. 3a and 3b) at a constant lateral spacing of 40–50 z^+ is evident. This minimum indicates that the instantaneous streamwise fluctuation at two points separated by the aforementioned distance is, on the average, opposite in time. Consequently, this distance corresponds to the mean spacing between neighboring high- and low-shear streaks. Hence, the lateral spacing between two low-shear or two high-shear streaks is supposed to be 80–100 z^+. The spanwise extension of the structures, which can be estimated from the findings in Fig. 4, shows to be on the order of magnitude predicted by the spanwise correlation of streamwise fluctuations $R_{\tau_x\tau_x}(z^+)$. Note that due to the limited lateral dimension of the sensor, only 125 z^+ could be resolved, such that only 2–3 neighboring streak structures could be captured.

The results clearly evidence that the low-speed fluid does not occur on a perfectly straight line in the streamwise direction, but rather resembles long meandering bands. It can further be evidenced that low-speed streaks split up into narrow bands or reassemble to form even more prominent structures of increased spanwise extension.

Similarly long features cannot be detected in the distributions of the spanwise wall shear stress when contour levels have been defined to represent the spanwise fluctuations (not shown). The footprints of meandering streaks, hairpin-vortex legs, counter-rotating vortices, and local sweeps will contribute differently to the temporal and spatial evolution of the spanwise wall shear-stress fluctuations than they do contribute to the distributions of the streamwise fluctuations, and only an in-depth investigation of the data will help to understand the difference. The apparent coherence of the spanwise fluctuations with drag-reducing effects, however, seems to indicate that the spanwise fluctuations, and hence the spanwise displacements of near-wall structures, play an important role in the generation process of turbulence production near the wall or are at least an important indicator of processes that are represented by changes in the spanwise component of the wall shear stress. Therefore, the investigation of the spanwise wall shear-stress fluctuations should be an important part of future studies.

The preceding findings are in good agreement with findings in higher regions of shear layers obtained from flow visualizations [3,4,30], near-wall hot-wire measurements [7], and observations in DNS data [20,21], to name only a few. These authors evidenced the existence of long meandering bands of low-speed fluid at wall distances of $5 < y^+ < 60$. Smith and Metzler [4] report meandering low-speed bands in turbulent boundary-layer flow at $Re_\Theta = 740$ to 5830 to eventually split up and to rejoin at some later instance. The bands possess streamwise length scales of $x^+ \geq 1000$. The authors further reported a high persistence of streaks, but they could not evidence them to be spatially fixed. They determined the spacing between identical streaks (i.e., between two neighboring low-speed or high-speed streaks) to be in the order of 100 z^+. Note that, different from the present wall shear-stress measurements, the results in higher regions of the shear layer show a rather balanced ratio of low- and high-speed zones. This is not surprising, because the skewness of the shear-stress fluctuations in the vicinity of the wall is reported to be about 0.8–1.0, whereas the velocity fluctuations in the logarithmic regions tend to have a skewness close to zero.

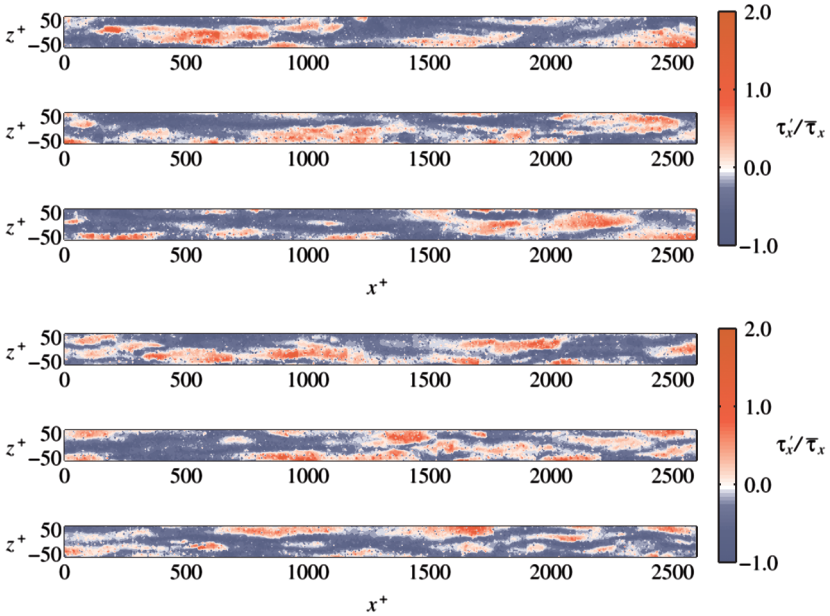

Fig. 4 Instantaneous wall shear-stress distribution in which each image possesses a field of view of $2500 \times 125\ l^+$ in the streamwise and spanwise directions, respectively. The contours indicate the instantaneous strength of the streamwise wall shear-stress fluctuations $\tau_x'/\bar{\tau}_x$.

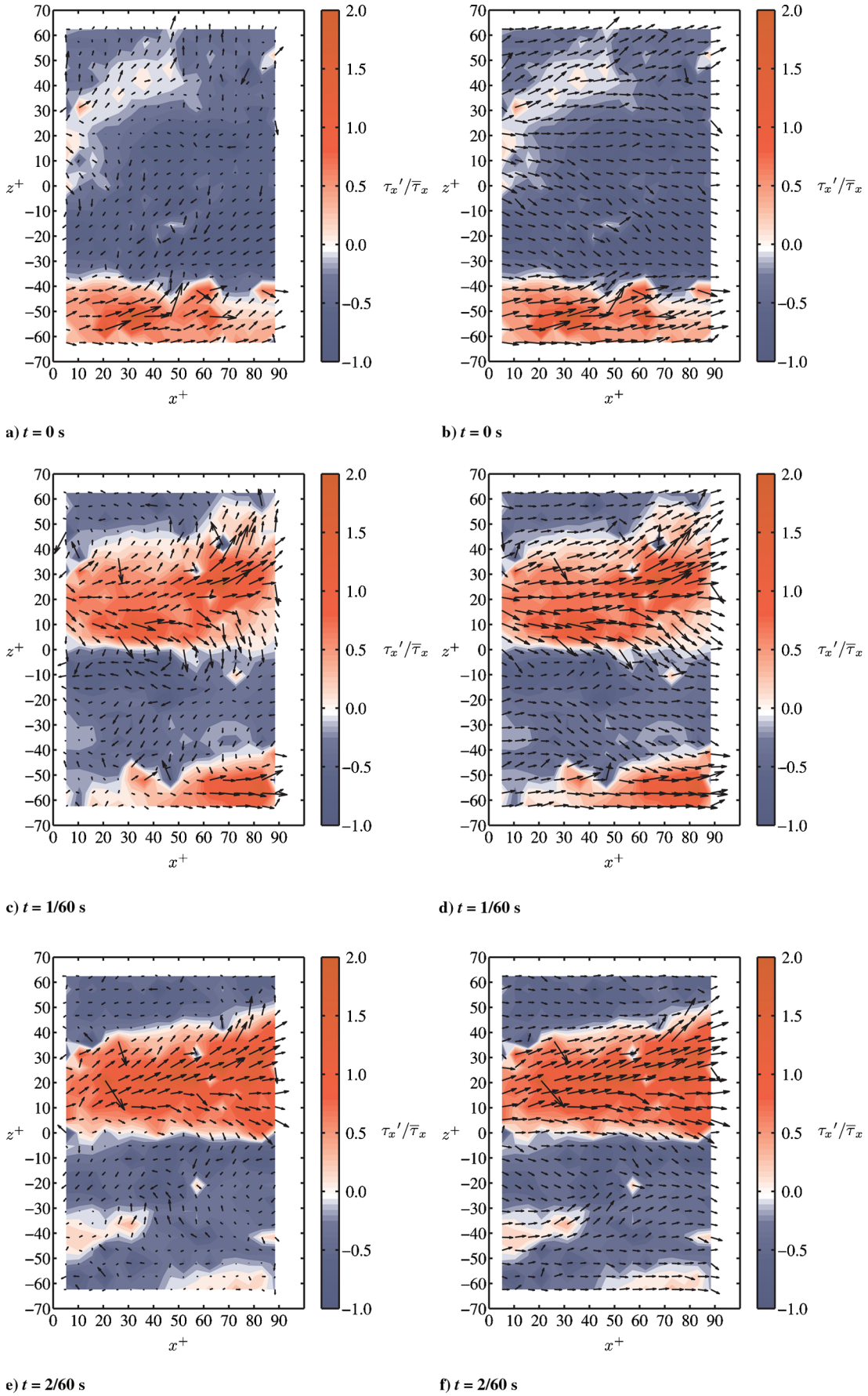

Fig. 5 Instantaneous two-dimensional wall shear-stress distributions at three consecutive time steps recorded with an array of micropillars consisting of 17 × 25 sensors along the streamwise and spanwise directions. Contours indicate the instantaneous strength of the streamwise wall shear-stress fluctuations $\tau_x'/\overline{\tau}_x$ (left). Vectors show the local streamwise and spanwise wall shear-stress fluctuations $\tau_x' = \tau_x - \overline{\tau}_x$ and τ_z', respectively, (right). Vectors show the local streamwise and spanwise wall shear stress τ_x and $\tau_z = \tau_z'$, respectively.

Instantaneous recordings of the wall shear-stress distribution at three consecutive recordings are given in Fig. 5. With the recording frequency during the measurements, the time between the samples is $1/60$ s, corresponding to $T^+ = 7.5$, normalized with inner variables (i.e., the friction velocity u_τ and the kinematic viscosity of the fluid ν). Contours indicate the instantaneous strength of the streamwise wall shear-stress fluctuations $\tau'_x/\bar{\tau}_x$. In Figs. 5a, 5c, and 5e, vectors indicate the local streamwise and spanwise wall shear-stress fluctuations $\tau'_x = \tau_x - \bar{\tau}_x$ and τ'_z, respectively. In Figs. 5b, 5d, and 5f, vectors show the local streamwise and spanwise wall shear stress τ_x and $\tau_z = \tau'_z$, respectively. The area corresponds to the dimension of the micropillar array (hence, approximately $90 \times 125\ l^+$ along the streamwise and spanwise directions, respectively).

Again, the spanwise coexistence of regions with low and high shear is clearly evident. The downstream convection of the turbulent structures can be observed from the consecutive sequence of recordings. The velocity at which the structures travel downstream corresponds to the convection velocity U_c, which can be determined from the temporal auto- and two-point correlation along the streamwise direction. However, the number of recorded images in the present experiments was insufficient to calculate the convection velocity. From measurements at a similar Reynolds number with a single sensor line aligned along the streamwise direction performed over much larger time spans, the convection velocity could successfully be determined and showed the value of $U_c = 10u_\tau$ to be a good first estimate.

IV. Conclusions

Measurements of the two-dimensional wall shear-stress distribution have been performed using the micropillar shear-stress sensor MPS^3. The preliminary statistics and the instantaneous fields of the wall shear-stress distribution evidence the near-wall region in turbulent flows to be characterized by an unbalanced distribution of streamwise low-shear and high-shear events. Low-speed streaks, the footprints of which are characterized by low values of the wall shear stress and are captured with the shear-stress sensor, are the dominant events in the vicinity of the wall. However, these streaks are interrupted from time to time by tempestuous high shear-stress values, most likely resulting from high-speed fluid originating from higher regions of the shear layer and being pushed toward the wall, causing a permanent coexistence of low- and high-shear regions. The high dynamic activity observed in the statistical characteristics of the wall shear-stress fluctuations confirm the flowfield within the viscous sublayer not to be "subject only to the turbulence as a boundary condition at its outer edge. Rather the sublayer and the adjacent wall region play an active role in the generation and preservation of turbulent shear flow" [31].

The low-shear regions evidenced in the experiments resemble long meandering bands interrupted by local high-shear-stress regions. A qualitative comparison evidences the structures detected in the present study to be similar to wall shear-stress distributions reported in the literature and to structures found in higher regions of the boundary layer [3–6].

The preliminary findings indicate the potential of the micropillar sensor concept to detect the multidirectional planar wall shear-stress distribution in turbulent flows. They evidence that the micropillar shear-stress sensor allows for a detailed investigation of the two-dimensional wall shear-stress distribution. The spatial resolution of the applied sensor array at the chosen Reynolds number has been shown to be chosen reasonably high to detect the spanwise dimensions of the dominant structures at an adequate resolution. The ability of the sensor to detect the two components of the wall shear stress will allow investigating the role of spanwise oscillations of near-wall structures in the regenerative process of near-wall turbulence.

The recording of the streamwise distribution will allow experimentally determining near-wall convection velocities of turbulent structures. The simultaneous assessment of time- and space-dependent data will make it possible to further investigate Taylor's hypothesis of frozen turbulence in flowfields, even with high fluctuation intensities, and will allow judging the degree to which streamwise spatial length scales can be correctly estimated from temporal scales.

The ability to detect the spanwise distribution of the wall shear stress will help to overcome ambiguities of single-point statistics in determining the correct geometric extensions of the large-scale coherent structures.

A further detailed discussion of the wall shear-stress characteristics and of the geometric properties of the streaklike structures is beyond the scope of this paper, and a more intrusive discussion needs to be done in the future on the basis of more comprehensive data, allowing for a proper statistical evaluation.

References

[1] Alfredsson, P. H., Johansson, A. V., Haritonidis, J. H., and Eckelmann, H., "The Fluctuating Wall-Shear Stress and the Velocity Field in the Viscous Sublayer," *Physics of Fluids*, Vol. 31, No. 5, 1988, pp. 1026–1033.
doi:10.1063/1.866783

[2] Heuer, W. D. C., and Marusic, I., "Turbulence Wall-Shear Stress Sensor for the Atmospheric Surface Layer," *Measurement Science and Technology*, Vol. 16, No. 8, 2005, pp. 1644–1649.
doi:10.1088/0957-0233/16/8/015

[3] Kline, S. J., Reynolds, W. C., Schraub, F. A., and Runstadler, P. W., "The Structure of Turbulent Boundary Layers," *Journal of Fluid Mechanics*, Vol. 30, No. 4, 1967, pp. 741–773.
doi:10.1017/S0022112067001740

[4] Smith, C. R., and Metzler, S. P., "The Characteristics of Low-Speed Streaks in the Near-Wall Region of a Turbulent Boundary Layer," *Journal of Fluid Mechanics*, Vol. 129, 1983, pp. 27.
doi:10.1017/S0022112083000634–54.

[5] Hutchins, N., and Marusic, I., "Evidence of Very Long Meandering Features in the Logarithmic Region of Turbulent Boundary Layers," *Journal of Fluid Mechanics*, Vol. 579, 2007, pp. 1.
doi:10.1017/S0022112006003946–28.

[6] Monty, J. P., Stewart, J. A., Williams, R. C., and Chong, M. S., "Large-Scale Features in Turbulent Pipe and Channel Flows," *Journal of Fluid Mechanics*, Vol. 589, 2007, pp. 147–156.
doi:10.1017/S002211200700777X

[7] Kreplin, H.-P., and Eckelmann, H., "Propagation of Perturbations in the Viscous Sublayer and Adjacent Wall Region," *Journal of Fluid Mechanics*, Vol. 95, No. 2, 1979, pp. 305–322.
doi:10.1017/S0022112079001488

[8] Taylor, G. I., "The Spectrum of Turbulence," *Proceedings of the Royal Society of London, Series A: Mathematical and Physical Sciences*, Vol. 164, 1938, pp. 476–490.
doi:10.1098/rspa.1938.0032

[9] Quadrio, M., and Luchini, P., "Integral Space Time Scales in Turbulent Wall Flows," *Physics of Fluids*, Vol. 15, No. 8, 2003, pp. 2219–2227.
doi:10.1063/1.1586273

[10] Lee, C., Kim, J., and Choi, H., "Suboptimal Control of Turbulent Channel Flow for Drag Reduction," *Journal of Fluid Mechanics*, Vol. 358, 1998, pp. 245–258.
doi:10.1017/S002211209700815X

[11] Yoshino, T., Suzuki, Y., and Kasagi, N., "Drag Reduction of Turbulence Air Channel Flow with Distributed Micro Sensors and Actuators," *Journal of Fluid Science and Technology*, Vol. 3, No. 1, 2008, pp. 137–148.
doi:10.1299/jfst.3.137

[12] Marusic, I., Kunkel, G. J., and Porté-Agel, F., "Experimental Study of Wall Boundary Conditions for Large-Eddy Simulation," *Journal of Fluid Mechanics*, Vol. 446, 2001, pp. 309–320.

[13] Kimura, M., Tung, S., Lew, J., Ho, C.-M., Jiang, F., and Tai, Y.-C., "Measurements of Wall Shear Stress of a Turbulent Boundary Layer Using a Micro-Shear-Stress Imaging Chip," *Fluid Dynamics Research*, Vol. 24, No. 6, 1999, pp. 329–342.
doi:10.1016/S0169-5983(99)00002-7

[14] Kimura, M., Takei, M., Ho, C.-M., Saito, Y., and Horii, K., "Visualization of Shear Stress with Micro Imaging Chip and Discrete Wavelet Transform," *Journal of Fluids Engineering*, Vol. 124, 2002, pp. 1018–1024.
doi:10.1115/1.1516599

[15] Miyagi, N., Kimura, M., Shoji, H., Saima, A., Ho, C.-M., Tung, S., and Tai, Y.-C., "Statistical Analysis on Wall Shear Stress of Turbulent Boundary Layer in a Channel Flow Using Micro-Shear Stress Imager," *International Journal of Heat and Fluid Flow*, Vol. 21, No. 5, 2000,

pp. 576–581.
doi:10.1016/S0142-727X(00)00047-3
[16] Große, S., and Schröder, W., "Mean Wall-Shear Stress Measurements Using the Micro-Pillar Shear-Stress Sensor MPS^3," *Measurement Science and Technology*, Vol. 19, No. 1, 2008, pp. 015403.
doi:10.1088/0957-0233/19/1/015403
[17] Große, S., and Schröder, W., "Dynamic Wall-Shear Stress Measurements in Turbulent Pipe Flow Using the Micro-Pillar Sensor MPS^3," *International Journal of Heat and Fluid Flow*, Vol. 29, No. 3, 2008, pp. 830–840.
doi:10.1016/j.ijheatfluidflow.2008.01.008
[18] Große, S., Soodt, T., and Schröder, W., "Dynamic Calibration Technique for the Micro-Pillar Shear-Stress Sensor MPS^3 ," *Measurement Science and Technology*, Vol. 19, No. 10, 2008, pp. 105201.
doi:10.1088/0957-0233/19/10/105201
[19] Hartnett, J. P., Koh, J. C. Y., and McComas, S. T., "A Comparison of Predicted and Measured Friction Factors for Turbulent Flow Through Rectangular Ducts," *Journal of Heat Transfer*, Vol. 84, No. 1, 1962, pp. 82–88.
[20] Kim, J., Moin, P., and Moser, R., "Turbulence Statistics in Fully Developed Channel Flow at Low Reynolds Number," *Journal of Fluid Mechanics*, Vol. 177, 1987, pp. 133–166.
doi:10.1017/S0022112087000892
[21] Moser, R. D., Kim, J., and Mansour, N. N., "Direct Numerical Simulation of Turbulent Channel Flow up to $Re_\tau = 590$," *Physics of Fluids*, Vol. 11, 1999, pp. 943–945.
doi:10.1063/1.869966
[22] Gavrilakis, S., "Numerical Simulation of Low Reynolds-Number Turbulent Flow Through a Straight Square Duct," *Journal of Fluid Mechanics*, Vol. 244, 1992, pp. 101–129.
doi:10.1017/S0022112092002982
[23] Lumley, J. L., *Stochastic Tools in Turbulence*, Academic Press, New York, 1970.
[24] Kim, J., and Hussain, F., "Propagation Velocity of Perturbations in Turbulent Channel Flow," *Physics of Fluids*, Vol. 5, No. 3, 1993, pp. 695–706.
doi:10.1063/1.858653
[25] Kreplin, H.-P., and Eckelmann, H., "Behavior of the Three Fluctuating Velocity Components in the Wall Region of a Turbulent Channel Flow," *Physics of Fluids*, Vol. 22, No. 7, 1979, pp. 1233–1239.
doi:10.1063/1.862737
[26] Khoo, B. C., Chew, Y. T., and Li, G. L., "Effects of Imperfect Spatial Resolution on Turbulence Measurements in the Very Near-Wall Viscous Sublayer Region," *Experiments in Fluids*, Vol. 22, No. 4, 1997, pp. 327–335.
doi:10.1007/s003480050055
[27] Obi, S., Inoue, K., Furukawa, T., and Masuda, S., "Experimental Study on the Statistics of Wall Shear Stress in Turbulent Channel Flows," *International Journal of Heat and Fluid Flow*, Vol. 17, No. 3, 1996, pp. 187–192.
doi:10.1016/0142-727X(96)00041-0
[28] Jeon, S., Choi, H., Yoo, J. Y., and Moin, P., "Space-Time Characteristics of the Wall-Shear Stress Fluctuations in a Low Reynolds-Number Channel Flow," *Physics of Fluids*, Vol. 11, No. 10, 1999, pp. 3084–3094.
doi:10.1063/1.870166
[29] Durst, F., Jovanovic, J., and Sender, J., "LDA Measurements in the Near-Wall Region of a Turbulent Pipe Flow," *Journal of Fluid Mechanics*, Vol. 295, 1995, pp. 305–335.
doi:10.1017/S0022112095001984
[30] Robinson, S. K., "Coherent Motions in the Turbulent Boundary Layer," *Annual Review of Fluid Mechanics*, Vol. 23, 1991, pp. 601–639.
doi:10.1146/annurev.fl.23.010191.003125
[31] Bakewell, H. P., Jr., and Lumley, J. L., "Viscous Sublayer and Adjacent Wall Region in Turbulent Pipe Flow," *Physics of Fluids*, Vol. 10, No. 9, 1967, pp. 1880–1889.
doi:10.1063/1.1762382

K. Asai
Associate Editor